Applied Catalysis B: Environmental 138–139 (2013) 219–228

Contents lists available at SciVerse ScienceDirect

Applied Catalysis B: Environmental

journal homepage: www.elsevier.com/locate/apcatb

Significant photocatalytic activity enhancement of titania inverse opals by anionic impurities removal in dye molecule degradation

Min Wu[a], Anmin Zheng[b], Feng Deng[b,**], Bao-Lian Su[a,c,d,*]

[a] Laboratory of Inorganic Materials Chemistry (CMI), University of Namur, Rue de Bruxelles 61, B-5000, Namur, Belgium
[b] Wuhan Centre for Magnetic Resonance, State Key Laboratory of Magnetic Resonance and Atomic and Molecular Physics, Wuhan Institute of Physics and Mathematics, Chinese Academy of Sciences (CAS), 430071, Wuhan, Hubei, China
[c] State Key Laboratory of Advanced Technology for Materials Synthesis and Processing, Wuhan University of Technology, Luoshi Road 1222, 430070, Wuhan, Hubei, China
[d] Department of Chemistry, University of Cambridge, Cambridge, United Kingdom

ARTICLE INFO

Article history:
Received 18 December 2012
Received in revised form 12 February 2013
Accepted 18 February 2013
Available online 28 February 2013

Keywords:
Inverse opal
TiO_2, Photocatalysis
Sulfate anion effect
Dye molecule degradation

ABSTRACT

The photocatalytic behavior in dye molecule degradation of highly ordered three dimensional macroporous titania inverse opals prepared by the polystyrene spheres templating method has been investigated. The sulfate impurity stemming from $K_2S_2O_8$ used as initiator for the styrene polymerization and remaining in the final materials in a form of sulfate anions was found to strongly inhibit the photocatalytic process of titania inverse opals. The mechanism of the negative effect of sulfate anionic impurity has been studied by the theoretical calculations and the comparison of samples subject to a wash process or not, the artificial addition of sulfate anions to the reaction medium and cycle experiments of samples without the washing process. Raman spectroscopy confirmed that in TiO_2 inverse opal structures, sulfate ions are present in divalent forms. However, in aqueous photocatalytic medium, monovalent hydrosulfate anions can also be present. Theoretical calculations on the interaction of sulfate (mono and divalent) anions and Rhodamine B (RhB) with TiO_2 inverse opal indicated that the adsorption binding energy of divalent sulfate anions on the titania surface (168 kcal/mol) is over four times as that of the Rhodamine B (36 kcal/mol) in the photocatalytic system and that of hydrosulfate anions is around 53–57 kcal/mol, still much higher than that of Rhodamine B. The strong adsorption of the anionic sulfate impurity on the surface of titania inverse opals would block the active sites and thus strongly affect the photocatalytic performance. A model of the negative action of sulfate anions has been proposed. This work leads to a new physic-chemical insight on the behavior of sulfate anions in the photocatalytic degradation of RhB and revealed that a single washing process to remove the impurity suggested significant promotion effect of the photocatalytic reaction without any surface modulations. This washing process dramatically suppressed the adsorption effect induced by the sulfate impurity and simplified the procedures, improving the photocatalytic performance.

1. Introduction

Titania has drawn intensive research attention since the discovery of photoinduced electrochemical splitting of water on a TiO_2 electrode in 1972 [1]. This led to wide number of applications of semiconductor photocatalysts in both energy and environmental categories, such as solar energy harvesting, sensors, environmental remediation, etc. [2–4]. Although a variety of chemical compositions [5] have been studied, TiO_2 remains the most popular photocatalyst owing to its high efficiency, low cost and non-toxicity. Currently, several methods have been developed to improve the photocatalytic activity of TiO_2, such as crystal structure properties control including the crystallite size and the crystalline phase [6]; anions [7] and cations [8] doping; variations of pore structures [9]; surface modification with graphene [10], and the addition of noble metals [11] and various band-gap semiconductors [12]. Moreover, the morphology control in inverse opals with three-dimensionally-ordered macroporous (3DOM) structures [13] has also been investigated.

The inverse opal structure, as it is termed, is derived from templates molding the opal structure assembled through various methods and compositions [14–17]. With the advancement of synthetic techniques, the inverse opaline porous structures could be

* Corresponding author at: Laboratory of Inorganic Materials Chemistry (CMI), University of Namur, Rue de Bruxelles 61, B-5000, Namur, Belgium.
Tel.: +32 0 81724531; fax: +32 0 81725414.
** Corresponding author.
E-mail addresses: dengf@wipm.ac.cn (F. Deng), bao-lian.su@fundp.ac.be (B.-L. Su).

0926-3373/$ – see front matter © 2013 Elsevier B.V. All rights reserved.
http://dx.doi.org/10.1016/j.apcatb.2013.02.044

patterned into multiple length scales from micropores to macropores [18]. It is most common that the uniform and spherical colloidal crystals are applied as templates due to their easy generation and high degree of periodicity in three dimensions. These 3D colloidal crystals reassemble into opals and a precursor of the defined chemical composition can be infiltrated into the interstitial space which will subsequently be converted to a solid phase. After the colloidal templates are removed, the interconnected voids in a solid skeleton are formed to give the inverse opal. A number of colloidal crystals including silica [14], polymer latex [15], gold [16] and semiconductor nanoparticles [17] have served as the templates while the polymer latex is used widely, as their preparation is easy and the removal by calcination is friendly to the wall composition. Recent studies on TiO_2 inverse opals showed exceptional photocatalytic performance of such macroporous structures in photodegradation of a series of pollutants [19] owing to the easy diffusion of pollutants and most importantly, to the photonic effect of highly ordered inverse opaline structures [20]. The obtained enhancement of the photocatalysis was promising which encouraged more scientists and engineers to explore such effects.

In the preparation of the polymer latex templates, persulfate typically served as the initiator in the polymerization process and also stabilized the latexes by the chemically bound sulfate groups of $SO_4^{\bullet -}$ initiating species derived from the decomposition of persulfate ions [21]. Most studies focus on the effect of pore size and the morphology control of inverse opal structures on the photocatalytic activity of TiO_2 inverse opals. Additionally, in these samples, the sulfate radicals obtained during the polymerization reaction can easily capture one electron to form anions and probably appear as a salt impurity after the polymer latex removal. This phenomenon can strongly affect the photocatalytic performance of TiO_2 inverse opals. It is possible that the photocatalytic activity measured without considering the effect of sulfate anions did not reflect the real photocatalytic behavior of the TiO_2 inverse opals. Unfortunately this effect of sulfate anions remaining in the inverse opals is often neglected.

In general, both anions and cations could affect the photooxidization rate by either competing with the pollutant by adsorbing on the photocatalyst surface, interfering with the electron-hole recombination rate or by scavenging the $^{\bullet}OH$ radicals. Though the majority of studies have shown the anions would interfere with the electron–hole recombination and enhance the photocatalysis [22], it was also reported that the anions have detrimental effects on the photocatalytic process. The negatively charged ions in the aqueous solution during photocatalysis would affect the adsorption of the pollutants by adsorbing onto the positively charged surface of TiO_2 particles while the number of active sites are decreased and the photocatalytic reaction rate would be influenced as a result [23]. Hence, in this work, the anionic sulfate impurity originating from the polymer templates during the inverse opal synthesis draws our attention. It is anticipated that a single step such as washing the TiO_2 inverse opal with water may remove the sulfate impurity and result in the modification of its photocatalysis performance. In order to study the effect of the sulfate impurity, we designed parallel experiments with the TiO_2 inverse opals with different pore diameters and calcination temperatures which are subject to different washing process and compared with those without washing treatment. The photocatalytic activity was performed in order to discover the effects of the anions from the impurities. Moreover, theoretical calculations were carried out to investigate the adsorption competition between the sulfate (divalent) and hydrosulfate (monovalent) anions and the dye, leading to the proposition of a model on the negative action of anionic sulfate (mono and divalent) species. The results indicated that the impurities strongly affect the photocatalysis and removing the impurity by washing the samples would greatly improve the photocatalytic activity. This work can provide the basic understanding on the behavior of sulfate anions in the photocatalytic dye degradation process and supply an efficient way to highly enhance the photocatalytic activity of TiO_2.

2. Experiment

2.1. Synthesis of titania inverse opal and removal of sulfate anionic impurity

The three dimensional titania inverse opals were prepared by the method previously reported [24]. Styrene was washed three times by 2 M NaOH beforehand in order to remove the impurities inhibiting the polymerization reaction. Three different sizes (350, 480 and 550 nm) of polystyrene spheres were obtained. Taking the 550 nm polystyrene spheres prepared and used in this work as an example, 15 mL of pre-washed styrene and 120 mL of water were heated to 70 °C in an oil bath under N_2 atmosphere. $K_2S_2O_8$ (0.14 g) was added as the initiator for the polymerization reaction. The reaction was stopped after 12 h by cooling the container. After the polystyrene (PS) spheres were obtained, the solvent was removed by drying in an oven at 60 °C. The precursor solution for infiltration was prepared by adding 1 mL hydrogen chloride acid (HCl), 5 mL titanium (IV) isopropoxide and 2 mL water in 5 mL ethanol and stirred for several minutes at room temperature. PS spheres were dispersed in a Buchner funnel with suction and then infiltrated with the precursor solution. The amount of precursor solution is equal to the template by mass. The mixture of precursor and template was air dried for 24 h. In order to illustrate the effect of the sulfate anionic impurity, some of the TiO_2 inverse opals were washed with water once after calcination to remove the impurity (washed sample was termed as "W550nm") by centrifuging for 6 h at 1500 rpm while the non-washed was kept for comparison (non-washed 550 nm spheres were termed as "NW550nm"). The template was then removed by calcinations in air with an increasing rate of 2 °C/min. The samples were calcined at 300 °C for 2 h, then at 400 °C for 2 h and finally at 550 °C for 2 h and were termed as "NW550nm550C" for the non-washed samples and "W550nm550C" for the washed, respectively. The samples which were subject to a further calcination at 700 °C for 2 h were termed as "NW550nm700C" and "W550nm700C" for non-washed and washed samples, respectively. For clarity, samples prepared using 350 nm polystyrene spheres with a washing procedure or not are named as follows: NW350nm550C and NW350nm700C for no washed samples calcined at 550 and 700 °C, respectively and W350nm550C and W350nm700C for washed samples calcined at 550 and 700 °C, receptively. All the other samples were synthesized using the same method with modified conditions (different sizes of polystyrene spheres) and termed accordingly. All the samples appeared visually as white powders.

2.2. Photocatalytic testing

0.05 g of highly ordered titania inverse opals was added to 50 mL Rhodamine B (RhB) with a concentration of 1×10^{-5} M. The suspension was poured in a quartz tube and inserted into a reactor under a UV lamp with the emission wavelength of 370 nm. The mixture was magnetically stirred at 700 rpm during the photocatalysis. A series of control experiments, adding 0.005 g of K_2SO_4 salt into the suspension, were carried out before the photocatalytic reaction was conducted using industrial sample P25 and the washed inverse sample (W350nm700C). An amount of ~0.75 mL aliquot was collected every specified time period after the photocatalysis began. All aliquots were centrifuged at 9000 rpm for

5 min to fully separate the solution from the powder and injected into the quartz cell for the UV–vis absorption spectrum measurements. For the cycle experiments, the suspension was centrifuged at 1500 rpm for 6 h after the photocatalysis. The degraded RhB solution was decanted after the centrifuge and the powder was dried at 60 °C for the next photocatalytic reaction cycle.

2.3. Characterizations

Powder X-ray diffraction patterns were collected using a Philips PW-170 diffractometer, equipped with a Cu anode X-ray tube (Cu Kα X-rays, λ = 1.5418 Å). Scanning electron microscopy (SEM) observations were carried out with a field-emission scanning electron microscopy (FE-SEM, JEOL JSM 7500). The UV–vis absorption spectra were obtained by Lamda 35 UV–visible spectrometer (Perkin Elmer Instruments). Raman spectroscopy was performed at room temperature in a Renishaw RM-1000 Raman spectrometer, employing an Ar^+ laser for excitation (λ = 514 nm).

2.4. Calculation method

Double numerical basis set with polarization functions (DNP) was used in all calculations. All calculations were performed by Dmol3 codes utilizing Lenovo7000 facilitated by the Supercomputing Center of Chinese Academy of Sciences [25].

3. Results and discussion

3.1. XRD analysis

The crystalline properties of all the samples prepared with three different sizes of polystyrene spheres (350 nm (Fig. 1a), 480 nm (Fig. 1b) and 550 nm (Fig. 1c)), non-washed (NW) and washed (W) and calcined at different temperatures were characterized by XRD technique as shown in Fig. 1. All the patterns show the typical anatase phase of TiO_2 whereas two small peaks at around 30° (2θ) present in all the non-washed samples. These two peaks have been identified as K_2SO_4 and it is probably originated from $K_2S_2O_8$ as the initiator used in the polystyrene synthesis. The styrene polymerization initiator persulfate which usually adsorbs on the surface of the styrene monomer decomposed into $SO_4^{\bullet -}$ free radicals when the styrene monomer solution was heated during the synthesis. These free radicals caught one of the electrons from the unstable carbon-carbon double bonds in the styrene monomer to initiate the polymerization reaction. It is very possible that after the air-drying and calcination process up to the point that the inverse opal was obtained, the $SO_4^{\bullet -}$ free radicals were probably turned into sulfate salts on the surface or mixed with the inverse opals which could be observed from the XRD patterns. It is estimated that sulfate ions represent about 5–10% (wt) in the sample. The K_2SO_4 salts impurity could affect significantly the photocatalytic activity, which is reflected in the photocatalysis study afterwards. The crystalline size could be calculated from the highest peak in the XRD pattern by Scherrer's equations [26]. The calculation shows the crystallite size of the non-washed and washed samples are similar if the synthesis condition is the same, indicating that washing treatment did not affect the crystallite size of TiO_2. This is essential that the effect of crystallite size on the photocatalytic activity of TiO_2 inverse opal can be eliminated and the behavior of sulfate anions in photocatalytic reactions can be deduced. The crystallite sizes are listed in Table 1. The nano-size particles would be beneficial for the photocatalytic reaction. Moreover, it is obvious that the washing step did not affect the crystal growth as expected. It is clear that the washing step can remove almost all the impurity while the crystalline phase remains anatase.

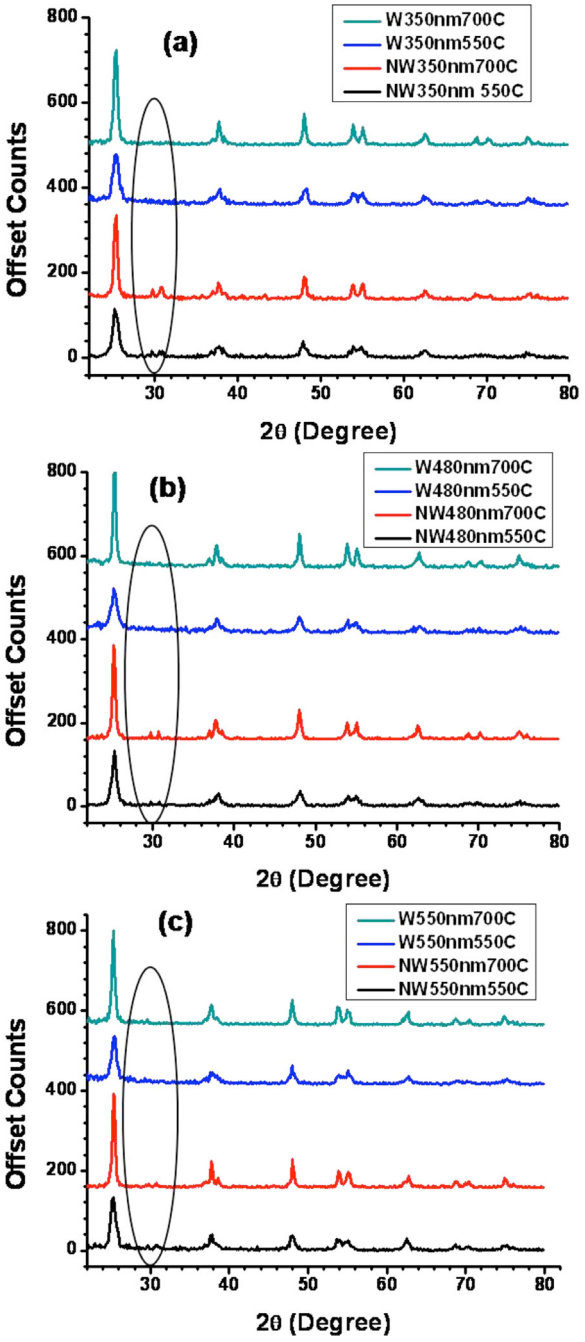

Fig. 1. XRD patterns of non-washed (NW-) and washed (W-) samples synthesized with different sizes of PS spheres: (a) 350 nm, (b) 480 nm and (c) 550 nm calcined at 550 °C and 700 °C respectively.

3.2. Raman spectroscopy

Raman spectroscopy was employed to further prove the impurity composition. Fig. 2 shows the Raman spectrum of the non-washed and washed samples prepared by 350 nm, 480 nm and 550 nm PS spheres, along with the typical spectrum of K_2SO_4 and $K_2S_2O_8$ for comparison. All the non-washed and washed samples exhibited peaks at ~394 cm^{-1}, ~513 cm^{-1} and ~637 cm^{-1}, which are assigned to anatase phase of titania. A small peak at ~981 cm^{-1} were observed in all the non-washed samples which are assigned to the asymmetric stretching mode S=O of SO_4^{2-}. The typical Raman spectrum of K_2SO_4 shows a strong signal at ~983 cm^{-1} while $K_2S_2O_8$ does not, suggesting the impurity composition is

Table 1
Summary of the crystal size and band-gap energy of the non-washed (NW-) and washed (W-) samples.

	NW350nm550C	NW350nm700C	W350nm550C	W350nm700C
Crystal size (nm) (±3 nm)	~12	~19	~11	~20
Band-gap energy (eV)	–	3.14	–	3.17
	NW480nm550C	NW480nm700C	W480nm550C	W480nm700C
Crystal size (nm)	~13	~18	~10	~22
Band-gap energy (eV)	–	3.16	–	3.20
	NW550nm550C	NW550nm700C	W550nm550C	W550nm700C
Crystal size (nm) (±3 nm)	~11	~19	~12	~20
Band-gap energy (eV)	–	3.15	–	3.18

K_2SO_4 as the XRD patterns revealed. Meanwhile, this small peak at ~981 cm^{-1} disappeared in all the washed samples indicating the washing process has removed the impurity successfully.

3.3. SEM analysis

According to previous studies, the inverse opal structure has positive effects on the photocatalytic activity [20]. Fig. 3 exhibits the typical SEM images of the non-washed and washed samples calcined at 700 °C using different diameters of PS spheres and it is observed that the washing step did not compromise the inverse opal structure since the inverse opals with highly ordered macropores and interconnected wall structures along with same periodic structures underneath are clearly observed. The pore size is measured to be approximately ~100 nm smaller than the original polystyrene spheres due to melting shrinkage during the calcinations. It was reported that the sulfate anions would induce the coagulation of titania nanoparticles and decrease the number of active sites [27], however, the coagulation effect was not observed in the SEM images of our samples.

3.4. UV–visible spectroscopy

The photonic properties were further characterized by UV–visible absorption spectroscopy. Fig. 4 presents the representative UV–vis absorption spectra of non-washed and washed

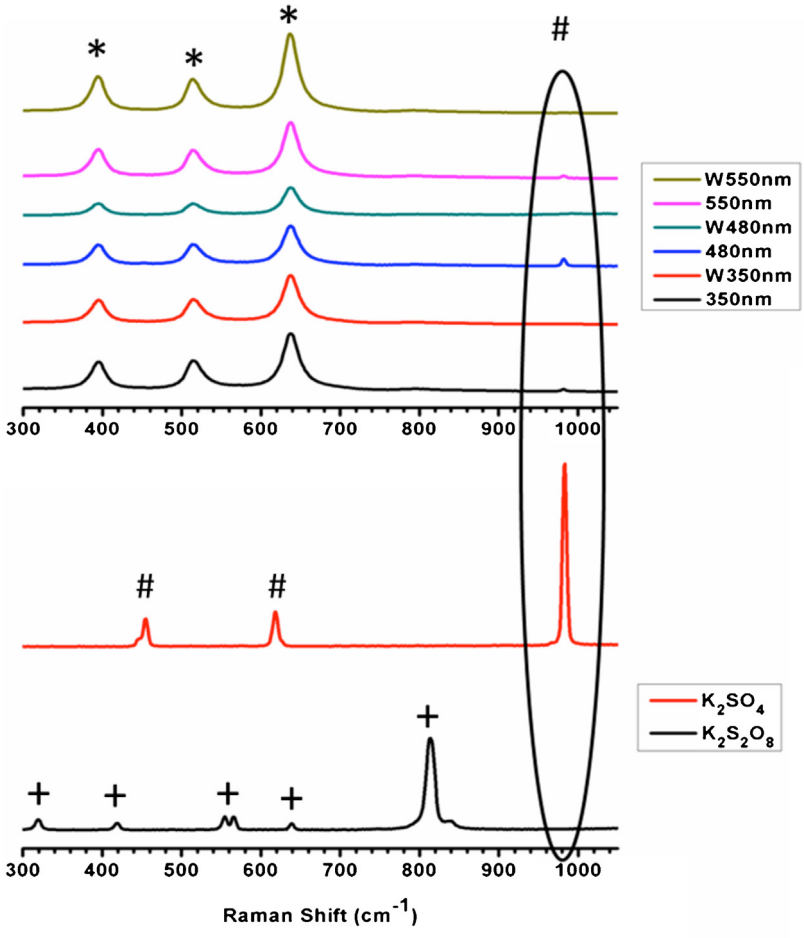

Fig. 2. Raman spectrum of non-washed (NW-) and washed (W-) samples synthesized with 350 nm, 480 nm and 550 nm PS spheres, in comparison with the typical Raman spectrum of K_2SO_4 and $K_2S_2O_8$ (*: anatase phase of TiO_2, #: K_2SO_4 phase and +: $K_2S_2O_8$ phase).

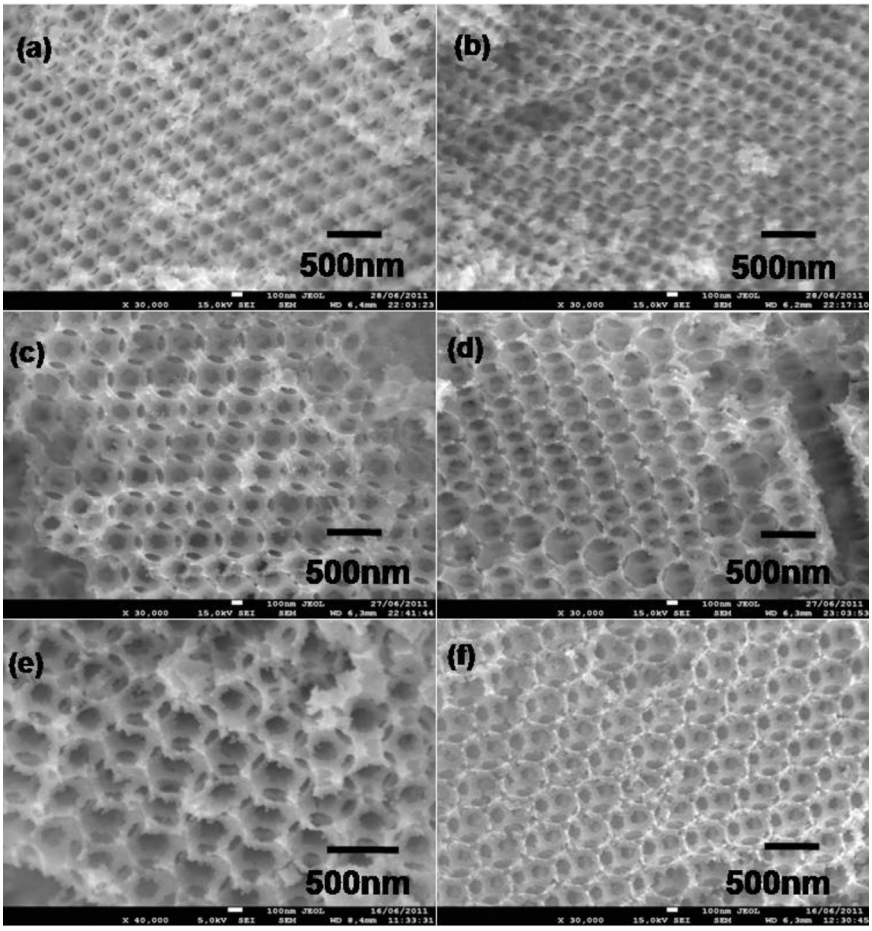

Fig. 3. Typical SEM images of the samples: (a) NW350nm700C; (b) W350nm700 C, (c) NW480nm700C, (d) W480nm700C, (e) NW550nm700C and (f) W550nm700C.

samples synthesized with different sized PS spheres at 700 °C. All the absorption spectra were obtained from the reflectance measurement. The band-gap energy can be estimated from the intersect point between the tangent line of the steep curve and the wavelength axis after the Kubelka–Munk transformation of the original reflectance data has been undertaken. This method is generally used to estimate the electronic band gap [28]. The transformed reflectance K was calculated from the equation below:

$$K = \frac{(1-R)^2}{2R}$$

R is the original reflectance. The wavelength has been converted to photon energy E_{phot} (eV). The value of $(K \times E_{phot})^{1/2}$ versus the photon energy E_{phot} was plotted and the band-gap energy was extrapolated from the tangent at the band edge. All the band-gap energy values calculated from Fig. 4 have been listed in Table 1. This study indicates that the band-gap energies of washed samples were shifted to shorter wavelengths which might be correlated to the photocatalytic performance afterwards. The sample with higher band-gap energy value usually has higher photocatalytic activity. This interesting correlation between the band-gap energy and photocatalysis was consistent with the phenomenon observed by our recent work [20] and deserves detailed investigation in future.

3.5. Photocatalytic activity

The photocatalysis study is essential to determine the effects of the impurity from the washing step. The photodegradation curves were plotted with C/C_0 vs reaction time "t". C_0 and C are the concentration of dye molecules in the reaction medium at the initial state (C_0) and after "t" minutes reaction (C), respectively. The sulfate anionic impurity is observed to be comparably high (~5%) in the total amount of the sample from the XRD pattern of the non-washed samples. Fig. 5 depicts the photodegradation curves of the non-washed sample compared with the washed samples synthesized with different sized PS spheres and calcination temperatures. It is obvious that the degradation occurred much faster for the washed samples compared to non-washed ones. Fig. 5(a)–(c) shows the same outcome for all the washed samples regardless of the size of the original PS spheres or the calcination temperatures. The photocatalytic performance of all the washed samples was greatly improved compared with the non-washed ones. The photocatalysis results suggest that the sulfate impurity did influence the photodegradation process and the washing step successfully suppressed the negative effect and promotes the photocatalytic performance.

During the dye photodegradation process, the sulfate anionic impurity could be dissolved in the solution while the generated doubly charged sulfate anions increased the ionic strength [27]. The sulfate anions could be rapidly adsorbed by the photocatalyst and block the active sites. The photocatalytic performance is therefore affected with a reduced number of active sites. In addition, it was reported that the anions would react with the surface holes and decrease the formation of •OH radicals resulting in a lower photodegradation rate [29].

In addition, whatever the size of the PS spheres was used, it always took less time for the samples calcined at 700 °C to fully degrade the dyes than those calcined at other temperatures due to

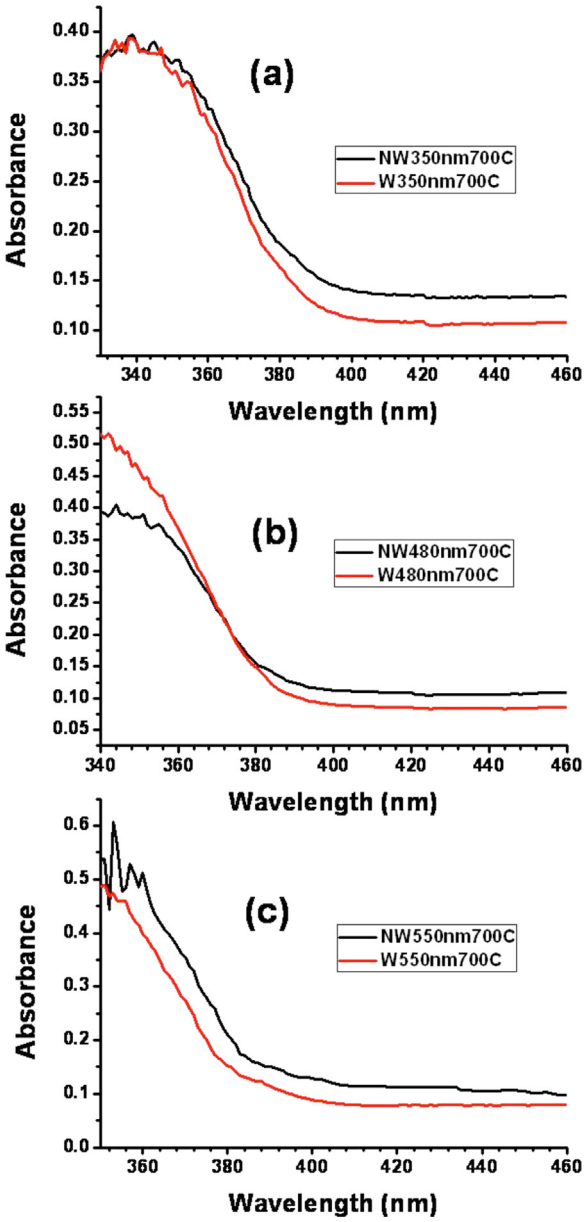

Fig. 4. The representative absorption spectrum of the non-washed and washed samples synthesized with different sized PS spheres at 700 °C: (a) NW350nm700C and W350nm700C; (b) NW480nm700C and W480nm700C; (c) NW550nm700C and W550nm700C.

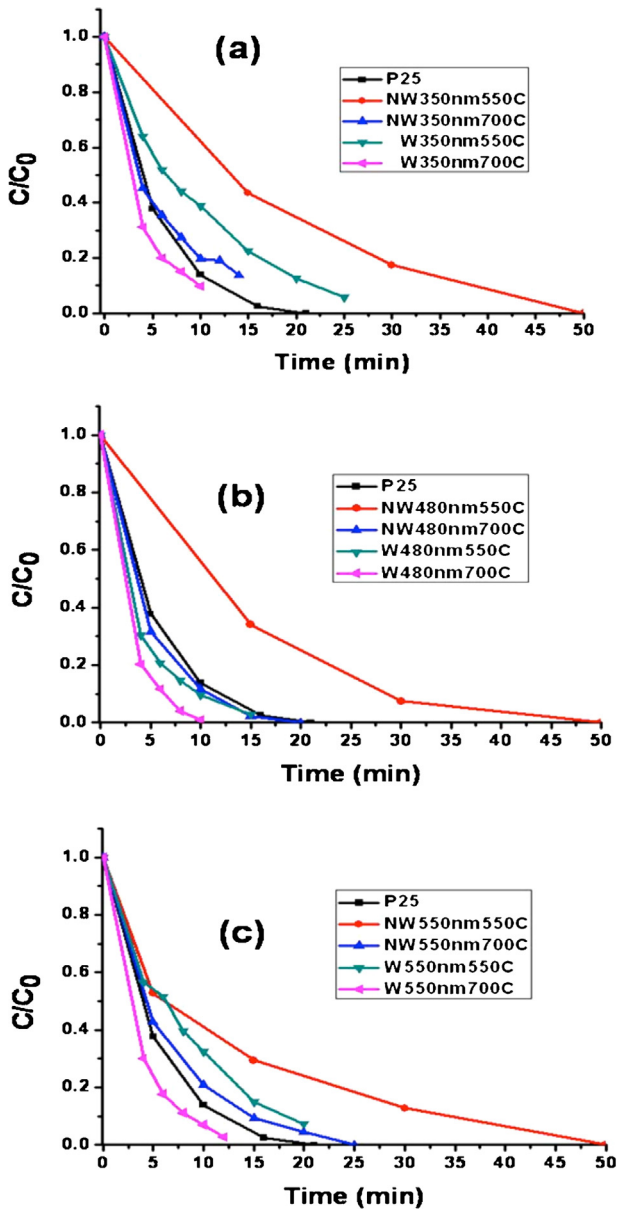

Fig. 5. The photodegradation curves of the non-washed and washed samples synthesized with different sized PS spheres and calcination temperatures: (a) NW350nm550C, NW350nm700C, W350nm550C and W350nm700C; (b) NW480nm550C, NW480nm700C, W480nm550C and W480nm700C; (c) NW550nm550C, NW550nm700C, W550nm550C and W550nm700C. All the samples are compared with the commercial product P25.

the fewer defects and better crystallinity in the structure, which was also observed in our previous report [20]. This tendency was well maintained even after the samples were washed. For comparison, the photocatalytic performance of the commercial product P25 is displayed in Fig. 5(a–c). All the washed samples calcined at 700 °C present a higher photocatalytic activity than P25.

The kinetics of the photoreaction were described as pseudo first order $\ln(C/C_0) = kt$. The degradation rate constant k was obtained from the plotting of $\ln(C/C_0)$ versus reaction time. Fig. 6 shows the first-order degradation rate constant k (min^{-1}) of all the samples calculated from Fig. 5 (The error is ±0.01). It is obvious that the washing process significantly stimulates photocatalysis and the washed samples reveal much higher degradation rate constants which were almost double the values of non-washed samples whatever the pore diameter of inverse opal was. Furthermore, the samples prepared by 480 nm PS spheres and calcined at 700 °C always possessed a higher degradation rate constant whether they were washed or not and showed the best photocatalytic performance among the samples prepared with three sizes of PS spheres, which may be assigned to the optimized pore size as reported previously and probably to the photonic effect [20]. The kinetics calculation further proves the positive effect of the washing process.

In order to further prove the effect of the sulfate impurity, a series of new experiments were carried out by adding K_2SO_4 salt to the reaction medium prior to the photocatalysis process using the industrial product P25 and the washed sample W350nm700 C titania inverse opal as photocatalysts since these two samples give the similar photodegradation rate constant. Fig. 7 compares the photodegradation rate constants of P25 and the washed sample W350nm700C before and after the sulfate salt was added. It is observed that the photodegradation rate constants of both

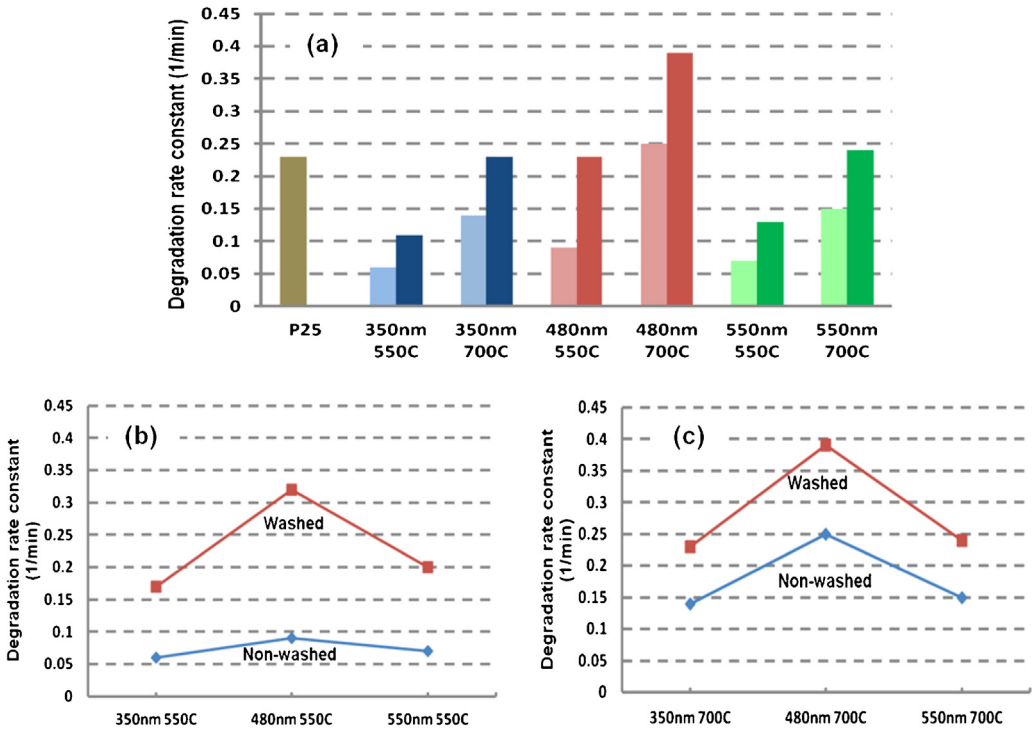

Fig. 6. (a) The photodegradation rate constant of the non-washed (light color) and washed (darker color) samples 350nm550C, 350nm700C, 480nm550C, 480nm700C, 550nm550C and 550nm700C compared with P25. (b) The photodegradation rate constant comparison of non-washed and washed samples synthesized from 350 nm, 480 nm and 550 nm PS spheres and calcined at 550 °C. (c) The photodegradation rate constant comparison of non-washed and washed samples synthesized from 350 nm, 480 nm and 550 nm PS spheres and calcined at 700 °C.

samples were decreased when the K_2SO_4 was added, which indicates the sulfate anions did affect the photodegradation process.

If the sulfate anions were only adsorbed on the titania surface after the electrons and holes were generated in the photocatalysis process, it is possible that after the photocatalysis reaction, these anions would be dissolved into the solution rather than stay on the surface of the titania. Hence, cycle experiments were conducted. Fig. 8 shows the photodegradation rate constants of P25 and the non-washed sample NW350nm700C after 3 photocatalysis cycles. As there is no sulfate impurity in the P25, the photodegradation process remains stable after 3 cycles as expected, while the case is different for the non-washed sample NW350nm700C. The photodegradation rate constants were gradually increased after each cycle (see Fig. 8). After the photocatalysis process, the sulfate impurity would be indeed dissolved in the solution rather than be readsorbed on the surface of the titania. After decanting the solution from the titania powder for the following cycle, the sulfate impurity was removed gradually and the negative effect was suppressed. The photodegradation performance was improved ultimately. Therefore, it was demonstrated by the cycle experiments that the negative effect of the sulfate anions resulted from the adsorption on the surface of the titania capturing the photo-generated holes and blocking active sites. The removal of these sulfate impurities would facilitate the photocatalytic reactions. However, if the washing process was not performed and even though the sulfate anions can be dissolved into the reaction solution, these anions are still present in the solution and affect negatively the photocatalytic performance of materials (Fig. 7). The removal of sulfate anions prior to the photocatalytic reaction is vital to guarantee the photocatalytic performance of TiO_2 inverse opals. It is possible that all the photocatalytic results reported in the literature using TiO_2 inverse opals without washing process are underevaluated.

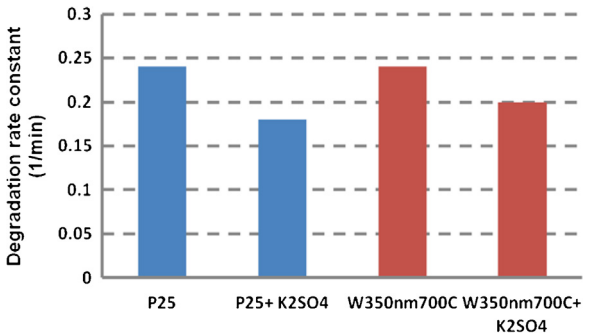

Fig. 7. The photodegradation rate constants of the P25 and the washed sample W350nm700C before and after the K_2SO_4 addition.

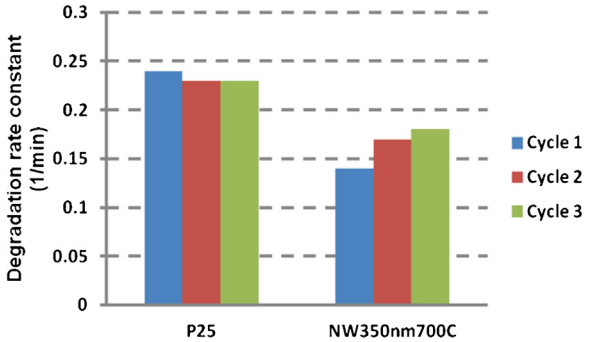

Fig. 8. The photodegradation rate constants of P25 and the non-washed sample NW350nm700C after 3 photocatalytic cycles.

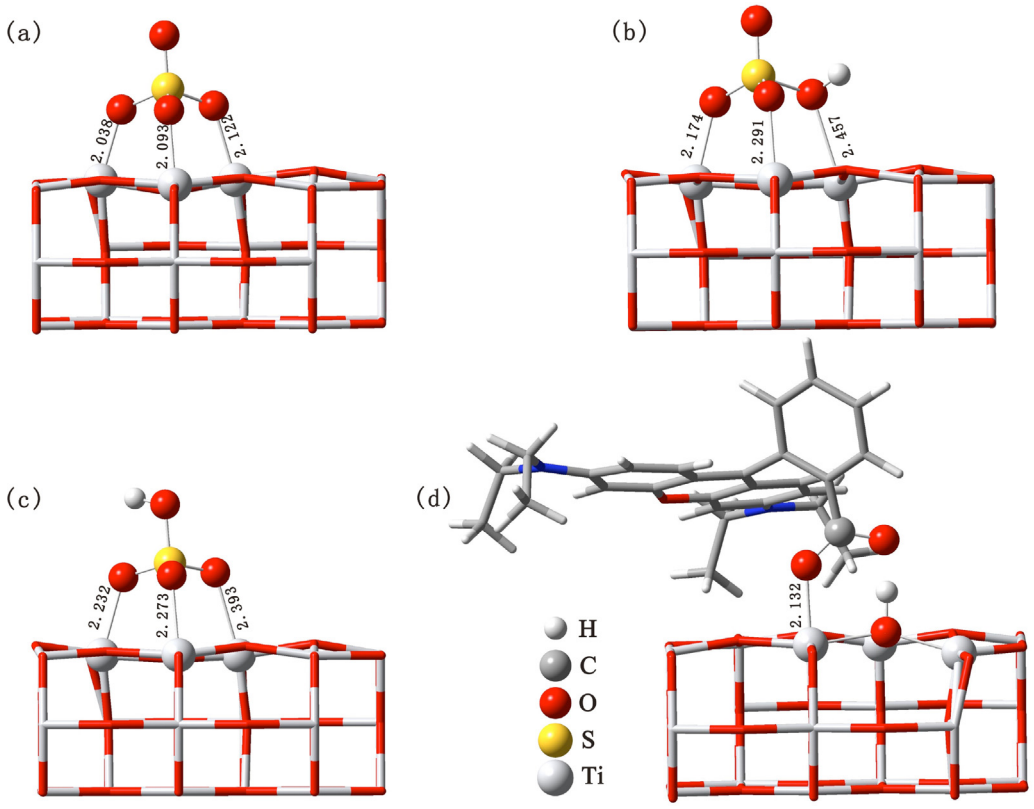

Fig. 9. Illustration images of theoretical calculations about the adsorption properties of SO_4^{2-} (a), HSO_4^- (b and c) and RhB (d) on the TiO_2 surface. Selected interatomic distances (in Å) are indicated.

3.6. Theoretical calculations

Experimental results suggested that the adsorption properties of SO_4^{2-} and RhB on the TiO_2 surface would strongly affect the photocatalytic performance. It is well known that the theoretical calculations are capable of predicting the adsorption structures and relevant energy parameters of solid catalysts [30,31]. Herein, the theoretical calculation was used to explore the properties of SO_4^{2-} and RhB adsorbed on the TiO_2. As shown in Fig. 9, a cluster containing 17Ti atoms was used in the theoretical calculations, and geometry optimizations were carried out by using density functional theory (DFT) at the generalized gradient approximation (GGA) level with the PBE (Perdew–Burke–Ernzerhof) exchange and correlation functional [32]. Double numerical basis set with polarization functions (DNP) was used in all calculations. All calculations were performed by Dmol3 codes utilizing Lenovo7000 facilitated by the Supercomputing Center of CAS [25].

During the photocatalytic reactions, the electrons are excited by the irridiation light from the valence band and migrated to the oxygen sites on the TiO_2 surface while the photogenerated holes remain in the titanium sites as the positively charged sites. For divalent SO_4^{2-} groups adsorption on the TiO_2 surface, SO_4^{2-} was binding to three oxygen sites (Fig. 9a), and the calculated Ti–O distances were 2.038, 2.093, and 2.122 Å, respectively. For the RhB adsorbed complexes on the TiO_2 surface (Fig. 9d), only one Ti–O bond has been formed with the bond length at 2.132 Å. On the adsorbed configuration, it is indicative that the interactions between the SO_4^{2-} group and TiO_2 will be stronger than the RhB on the TiO_2. The binding energy (BE) was defined the energy difference between the adsorbed complex system and the sum of the individual fragments. We also used BE to quantitatively evaluate the adsorbed strength of SO_4^{2-} group and RhB on the surface of TiO_2. On the basis of the optimized adsorbed structure, the BE of SO_4^{2-} group on the surface of TiO_2 is 168 kcal/mol, which is about four time of the BE for the RhB interacted with the TiO_2 surface (36 kcal/mol). It is well known that the interaction energy of the sulfate ions is rather strongly affected by the charge. Considering that SO_4^{2-} is a base and although Raman spectrscopy confirmed that in solid state of TiO_2 inverse opal structures, sulfate ions are present in divalent form, in aqueous solution where the photocatalytic reaction occurs, monovalent HSO_4^- anions can be also present. The structures HSO_4^- on the TiO_2 surface are also optimized as shown in Fig. 9b and c. Comparing with SO_4^{2-} group, Ti-O bond length of HSO_4^- on the TiO_2 surface are increased to 2.2–2.5 Å, indicative of relatively weak interaction between HSO_4^- and TiO_2 surface. On the basis of the adsorbed conformations, the binding energies of HSO_4^- on the TiO_2 are 53–57 kcal/mol. Obviously, the host/guest interactions between HSO_4^- and TiO_2 surface are considerably lower than the one of SO_4^{2-} group (168 kcal/mol), however, it is also much larger than RhB interacted with the TiO_2 surface (36 kcal/mol)

High binding energy of SO_4^{2-} on the TiO_2 surface indicated that the adsorption of RhB in the photocatalytic reaction would be significantly interfered and the photocatalytic performance becomes poorer as a result. Though the SO_4^{2-} is strongly adsorbed on the TiO_2 surface, this chemical adsorption occurs on the basis of photogenerated holes formation inducing positively charged Ti sites. Fig. 10 shows the schematic mechanism of the adsorption interference by sulfate anions. Thereby, it is anticipated that when the photocatalytic reactions finish and electric charges reach the equilibrium, the interaction between the sulfate anions and water tends to be dominant and these sulfate impurities could be easily removed to suppress the adsorption interference. Previous study even found that sulfate anions would affect the adsorption of

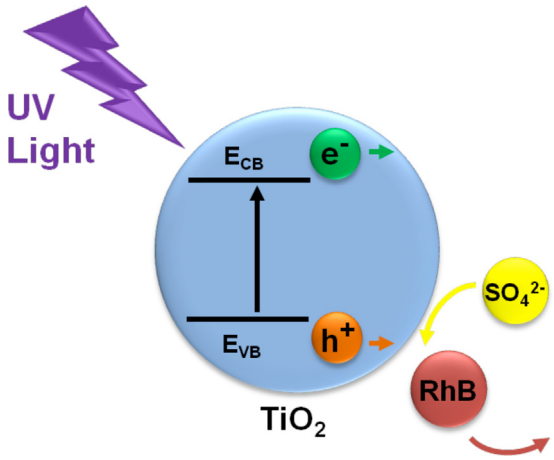

Fig. 10. Schematic image of the adsorption interference by sulfate anions during the RhB photodegradation reaction.

phenol on the TiO_2 surface in the darkness [23]. However, the detrimental effect of the sulfate anions on the adsorption property during the photocatalytic reactions is considered to be dominant in the RhB photodegradation process.

The negative effect of sulfate anions on the photocatalytic activity of TiO_2 was previously reported and attributed this to the coagulation effect of TiO_2 nanoparticles during the calcination process since the sulfate anions can be considered as an initiator of the coagulation of TiO_2 nanoparticles. However, this coagulation effect has not been observed (SEM pictures in Fig. 3). Our present study disclosed clearly that the negative effect of sulfate anions is due to sulfate anions masking active sites, blocking the photocatalytic process by capturing the photogenerated holes.

4. Conclusion

Titania inverse opals were synthesized by the templating method from polystyrene spheres of different sizes of 350, 480 and 550 nm and calcined at different temperatures. A washing step was added after the calcination of the inverse opals in order to check the effect of sulfate anions originating from $K_2S_2O_8$ as the polymerization initiator. Both the XRD patterns and Raman spectrum show the washing process has removed almost all the sulfate impurity and maintained the crystal structure property well. Meanwhile, the SEM images also show the inverse opal structure was properly preserved after washing. Photocatalysis study indicates that after removing the anionic sulfate impurity by the washing process, the photocatalytic performance was significantly improved. The negative effect of sulfate anions is due to the coverage of sulfate anions on active sites, blocking the photocatalytic process by capturing the photogenerated holes. Theoretical calculations revealed the stronger adsorption of sulfate anions on the TiO_2 surface than the RhB dye during the holes photogeneration and further proved the significant adsorption interference by sulfate anions. This study indicates that a simple washing process could suppress the detrimental effect which might open an easy path to promote the photocatalysis in the future.

Acknowledgements

This work was carried out in the framework of an Interuniversity Attraction Poles Program (Inanomat-P6/17)-Belgium State-Belgian Science Policy and the project "Redugaz", financially supported by the European community and the Walloon government in the framework of Interreg IV (France-Wallonie) and the National Natural Science Foundation of China (21073228). B.L. Su acknowledges the Chinese Central Government for an "Expert of the State" position in the program of a "Thousand talents" and the Chinese Ministry of Education for a Changjiang Scholar position at the Wuhan University of Technology. B. L. Su also thanks Clare Hall College at the University of Cambridge for a Life Membership and the Department of Chemistry (Grey's group) for financial support.

References

[1] A. Fujishima, K. Honda, Nature 238 (1972) 37–38.
[2] A.L. Linsebigler, G. Lu, J.T. Yates Jr., Chemical Reviews 95 (1995) 735–738.
[3] A. Hagfeldt, M. Gratzel, Chemical Reviews 95 (1995) 49–68.
[4] A. Mills, S. Le Hunte, Journal of Photochemistry and Photobiology A 108 (1997) 1–35.
[5] D.S. Bhatkhande, V.G. Pangarkar, A.A.C.M Beenackers, Journal of Chemical Technology and Biotechnology 77 (2002) 102–116.
[6] (a) Z. Zhang, C. Wang, R. Zakaria, J.Y. Ying, Journal of Physical Chemistry B 102 (1998) 10871–10878;
(b) S.Y. Chae, M.K. Park, S.K. Lee, T.Y. Kim, S.K. Kim, W.I. Lee, Chemistry of Materials 15 (2003) 3326–3331;
(c) I. Roger, T. Bickley, J.S. Gonzalez-Carreno, L. Lees, R.J.D. Palmisano, J. Tilley, Solid State Communications 92 (1991) 178–190.
[7] N. Serpone, Journal of Physical Chemistry B 110 (2006) 24287–24293.
[8] M.R. Hoffmann, S.T. Martin, W. Choi, D.W. Bahnemann, Chemical Reviews 95 (1995) 69–96.
[9] (a) Q. Dai, Y. Shi, Y.G. Luo, J.L. Blin, D.J. Li, C.W. Yuan, B.L. Su, Journal of Photochemistry and Photobiology A 148 (2002) 295–301;
(b) X.C. Wang, J.C. Yu, C. Ho, Y.D. Hou, X.Z. Fu, Langmuir 21 (2005) 2552–2559;
(c) X.F. Chen, X.C. Wang, X.Z. Fu, Energy and Environmental Science 2 (2009) 872–877;
(d) X.Y. Li, L.H. Chen, Y. Li, J.C. Rooke, C. Wang, Y. Lu, A. Krief, X.Y. Yang, B.L. Su, Journal of Colloid and Interface Science 368 (2012) 128–138;
(e) X.Y. Li, L.H. Chen, J.C. Rooke, Z. Deng, Z.Y. Hu, S.Z. Huang, L. Wang, Y. Li, A. Krief, X.Y. Yang, B.L. Su, Journal of Colloid and Interface Science 394 (2013) 252–262.
[10] (a) W. Graeme, B. Seger, V.K. Prashant, ACS Nano 2 (2008) 1487–1491;
(b) H. Zhang, X.J. Lv, Y. Wang, J.H. Li, ACS Nano 4 (2010) 380–386.
[11] (a) V. Subramanian, E.E. Wolf, P.V. Kamat, Journal of the American Chemical Society 126 (2004) 4943–4950;
(b) Y. Xie, K.L. Ding, Z.M. Liu, R.T. Tao, Z.Y. Sun, H.Y. Sun, H.Y. Zhang, G.M. An, Journal of the American Chemical Society 131 (2009) 6648–6649.
[12] I. Robel, V. Subramanian, M. Kuno, P.V. Kamat, Journal of the American Chemical Society 128 (2006) 2385–2393.
[13] A. Stein, F. Li, N.R. Denny, Chemistry of Materials 20 (2008) 649–666.
[14] J.S. King, E. Graugnard, C.J. Summers, Advanced Materials 17 (2005) 1010–1013.
[15] (a) B.T. Holland, C.F. Blanford, A. Stein, Science 281 (1998) 538–540;
(b) A. Stein, Microporous and Mesoporous Materials 44–45 (2001) 227–239.
[16] P.C. Ohara, D.V. Leff, J.R. Heath, W.M. Gelbart, Physical Review Letters 75 (1995) 3466–3469.
[17] L. Huang, Z. Wang, J. Sun, L. Miao, Q. Li, Y. Yan, D. Zhao, Journal of the American Chemical Society 122 (2000) 3530–3531.
[18] F. Muldarisnur Marlow, P. Sharifi, R. Brinkmann, C. Mendive, Angewandte Chemie International Edition 48 (2009) 6212–6233.
[19] (a) F. Sordello, C. Duca, V. Maurino, C. Minero, Chemical Communications 47 (2011) 6147–6149;
(b) M. Srinivasan, T. White, Environmental Science and Technology 41 (2007) 4405–4409.
[20] (a) J.I.L. Chen, G. von Freymann, S.Y. Choi, V. Kitaev, G.A. Ozin, Advanced Materials 18 (2006) 1915–1919;
(b) J.I.L. Chen, G.A. Ozin, Journal of Materials Chemistry 19 (2009) 2675–2678;
(c) A. Mihi, H. Miguez, Journal of Physical Chemistry B 109 (2005) 15968–15976;
(d) S.H.A. Lee, N.M. Abrams, P.G. Hoertz, G.D. Barber, L.I. Halaoui, T.E. Mallouk, Journal of Physical Chemistry B 112 (2008) 14415–14421;
(e) M. Wu, Y. Li, Z. Deng, B.L. Su, ChemSusChem 4 (2011) 1481–1488;
(f) Y. Li, F. Piret, T. Léonard, B.L. Su, Journal of Colloid and Interface Science 348 (2010) 43–48;
(g) F. Piret, B.L. Su, Chemical Physics Letters 454 (2008) 318–322;
(h) Y. Li, Z.Y. Fu, B.L. Su, Advanced Functional Materials 22 (2012) 4634–4667.
[21] G. Odian, The Principles of Polymerization, John Wiley & Sons, Inc., Hoboken, New Jersey, USA, 2004.
[22] K. Kabra, R. Chaudhary, R.L. Sawhney, Industrial and Engineering Chemistry Research 43 (2004) 7683–7696.
[23] A.A. Yawalkar, D.S. Bhatkhande, V.G. Pangarkar, A.A.C.M. Beenackers, Journal of Chemical Technology and Biotechnology 76 (2001) 363–370.
[24] R.C. Schroden, M. Al-Daous, C.F. Blanford, A. Stein, Chemistry of Materials 14 (2002) 3305–3315.
[25] B. Delley, Journal of Chemical Physics 113 (2000) 7756–7764.
[26] H. Borchert, E.V. Shevchenko, A. Robert, I. Mekis, A. Kornowski, G. Grubel, H. Weller, Langmuir 21 (2005) 1931–1936.

[27] K.E. O'Shea, E. Pernas, J. Saiers, Langmuir 15 (1999) 2071–2076.
[28] K.M. Reddy, S.V. Manorama, A.R. Reddy, Materials Chemistry and Physics 78 (2002) 239–245.
[29] Y.G. Adewuyi, Environmental Science and Technology 39 (2005) 8557–8570.
[30] H. Zhang, A. Zheng, H. Yu, S. Li, X. Lu, F. Deng, Journal of Physical Chemistry C 112 (2008) 15765–15770.
[31] N. Feng, A. Zheng, S. Huang, H. Zhang, N. Yu, C. Yang, S. Liu, F. Deng, Journal of Physical Chemistry C 114 (2010) 15464–15472.
[32] J.P. Perdew, K. Burke, M. Ernzerhof, Physical Review Letters 77 (1996) 3865–3868.